Heinonen, Juha; Pasanen, Toni; Vähänissi, Ville; Juntunen, Mikko; Savin, Hele

Modeling Field-effect in Black Silicon and its Impact on Device Performance

Published in:
IEEE Transactions on Electron Devices

DOI:
10.1109/TED.2020.2975145

Published: 01/04/2020

Document Version
Peer reviewed version

Please cite the original version:
Heinonen, J., Pasanen, T., Vähänissi, V., Juntunen, M., & Savin, H. (2020). Modeling Field-effect in Black Silicon and its Impact on Device Performance. *IEEE Transactions on Electron Devices*, *67*(4), 1645-1652. [9027860]. https://doi.org/10.1109/TED.2020.2975145

Modeling Field-effect in Black Silicon and its Impact on Device Performance

Juha Heinonen, Toni P. Pasanen, Ville Vähänissi, Mikko A. Juntunen, and Hele Savin

***Abstract*— Black silicon (b-Si) has improved the performance of solar cells and photodetectors due to the excellent optics and surface passivation achieved with atomic-layer-deposited (ALD) dielectric films. One major reason for the success is the strong field-effect caused by the high density of fixed charges present in the dielectric. Depending on the device, the field-effect can be utilized also in a more active role than for mere surface passivation, including formation of floating and/or induced junctions in silicon devices. However, in order to utilize the field-effect efficiently, deeper understanding on thin film charge-induced electric field and its effects on charge carriers in b-Si is required. Here we investigate the field-effect in b-Si using Silvaco Atlas semiconductor device simulator. By studying the electric field and charge carrier profiles, we develop a model where the electrical properties of b-Si can be approximated with a planar surface, which significantly simplifies device level simulations. We validate the model by simulating the spectral response of a b-Si induced junction photodiode achieving less than 1% difference compared to experimental device performance in a wide range of wavelengths. Finally, we apply the model to study how variation in surface recombination velocity affects the short wavelength sensitivity and dynamic range in a b-Si photodiode.**

***Index Terms*—atomic layer deposition, black silicon, field-effect, photodiode, simulation**

I. Introduction

BLACK silicon (b-Si), i.e. a nanostructured silicon surface, has recently been demonstrated to significantly enhance the performance of silicon-based optoelectronic devices, such as solar cells and photodiodes, due to its excellent optical properties [1]–[4]. However, the excellent optics alone does not guarantee high performance, but the electrical properties are equally important. Consequently, especially due to the increased surface area, the reduction of charge carrier recombination via efficient surface passivation is of utmost importance in b-Si devices. This is typically achieved by a thin film that is commonly deposited on nanostructured surfaces by atomic layer deposition (ALD). It is well known that efficient surface passivation requires both high-quality interface between the thin film and silicon and a strong field-effect. In the case of b-Si, the latter is emphasized [5]. The field-effect is achieved by a sufficient amount of electric charge incorporated in the film, which is the case e.g. in ALD aluminum oxide Al_2O_3 [5]. Indeed, the material has been demonstrated to provide excellent passivation of b-Si surfaces [6], [7], resulting in e.g. high-performing solar cells [3], [8], [9].

In addition to surface passivation, the field-effect can be utilized also in a more active role depending on the device. For instance in interdigitated back contact (IBC) solar cells, the field-effect can be utilized to form a front floating emitter (FFE), which reduces losses caused by transversal transport of minority carriers to the rear emitter [10], [11]. Another example, where the field-effect is even more critical is a b-Si photodetector with an induced junction [4], [12]. There it is used to form the charge carrier-collecting p-n junction, i.e. the most important part of the whole device. In such device, the field-effect allows to omit conventionally-used ion-implanted p-n junction, which reduces both Auger and Shockley-Read-Hall recombination [4], and hence, enhances the device performance.

As the above examples demonstrate, different applications set differing requirements for the properties of the thin film used to induce the field-effect. Hence, in order to utilize the field-effect efficiently and to understand, which factors are important for various applications, deeper understanding on thin film charge-induced electric field and its effects on charge carriers in b-Si is required. One of the most effective ways to pursue this objective is to simulate the electric field in the b-Si nanostructures. However, due to the minuscule size of b-Si, and hence, an enormous number of individual nanostructures on the device surface, simulation of b-Si structures directly on device level is slow and impractical.

Here we address the above challenges by developing a planar equivalent model for b-Si coated with a charged thin film and study the field-effect in nanostructured devices. The results are analyzed mainly from the perspective of induced junction b-Si photodiodes, which set the most demanding requirements for the field-effect. Nevertheless, the results are applicable also to

The authors acknowledge Business Finland project RADI for financial support. The authors acknowledge the provision of facilities and technical support by Aalto University at OtaNano – Micronova Nanofabrication Centre. The authors from Aalto University are part of Academy of Finland Flagship Programme, Photonics Research and Innovation (PREIN). Antti Haarahiltunen is acknowledged for help in result analysis of this work. "J. Heinonen and T. P. Pasanen acknowledge the financial support of the Aalto ELEC Doctoral School. T. P. Pasanen acknowledges Jenny and Antti Wihuri Foundation, Walter Ahlström Foundation, and the Foundation of Electronics Engineers for the financial support.

J. Heinonen, T. P. Pasanen, V.Vähänissi, and H. Savin are with the Department of Electronics and Nanoengineering, Aalto University, Espoo 02150, Finland (e-mail: juha.heinonen@aalto.fi, toni.pasanen@aalto.fi, ville.vahanissi@aalto.fi, hele.savin@aalto.fi). J. Heinonen is also with ElFys, Inc., Espoo 02150, Finland. M. A. Juntunen was with the Department of Electronics and Nanoengineering, Aalto University, Espoo 02150, Finland. He is now with ElFys, Inc., Espoo 02150, Finland (e-mail: mikko.juntunen@elfys.fi).

other devices with less stringent requirements for the field-effect, such as IBC solar cells. The simulations first concentrate on carrier concentration and electric field distribution inside and in the vicinity of the nanostructures. More specifically, we study the effect of substrate resistivity on the field-effect with a typical charge density found in ALD thin films applied on the surface. Later, also the charge density in the dielectric is varied to investigate the limits for efficient use of field-effect in b-Si and to search for boundary conditions of the planar model. The model is then applied on device level, and the simulated quantum efficiency (QE) is compared to an experimentally-determined QE of a b-Si photodiode to validate the model. Finally, to demonstrate the utilization of the developed model, the effect of thin film – Si interface quality and light intensity on the QE of the device is studied using the model.

II. Model for Field-Effect in b-Si

A. Typical b-Si Structure Coated With a Thin Film

A typical structure used in electrical b-Si devices that consists of nanostructures covered with a conformal thin film was selected as a starting point. A scanning electron microscope (SEM) image of such structure is presented in Fig. 1a. Using similar structure, reflectance less than 1 % combined with low surface recombination velocity (SRV) of <10 cm/s has earlier been demonstrated experimentally [5], [6]. The efficient reduction of surface reflectance by b-Si is due to the minuscule size of the nanostructures: since the dimensions of b-Si are in the range of the wavelength of light, b-Si functions as a graded refractive index layer and no clear interface between air and silicon exists [1], [13]. The nanostructure imaged in Fig. 1a is fabricated by inductively-coupled plasma reactive ion etching (ICP-RIE) method, which enables to adjust the b-Si morphology extensively [2] and produces no lattice damage [5] or contamination, opposite to other b-Si fabrication methods, such as metal-assisted chemical etching [14] or laser treatment [15]. As was mentioned earlier, electrical devices usually require that the surface is covered with a thin film to reduce charge carrier recombination. This is critical especially in the case of b-Si due to its increased surface area. The thin film is often deposited with ALD to obtain good conformality and to form a high-quality interface with silicon. Additionally, the film should contain sufficient amount of fixed charges to passivate the surface efficiently and, in the extreme case, to induce a carrier-collecting p-n junction.

A schematic of the corresponding structure used in the simulations is presented in Fig. 1b. It consists of four 700 nm tall and 200 nm wide evenly spaced silicon needles, similar to [5]. The needle tips are slightly flattened (tip width 20 nm) to mimic the actual shape of the nanostructure. In reality, the shape and position of the needles are somewhat random [2], but the structure used here represents an approximated average of several needles. Additionally, a 2 µm deep region of high-quality silicon below the needles is included in the simulation structure to represent the substrate.

The thin film is selected here to be a 20 nm thick ALD Al_2O_3, which contains a local charge density of -2.5×10^{12} cm^{-2} along the Si-Al_2O_3 interface, according to [4]. In general, the Al_2O_3 layer could be replaced in the model with any other dielectric with suitable charge polarity and density. The selection of ALD Al_2O_3 as the thin film material is justified by the wide availability of experimental data on its properties and the resulting performance of various devices [3], [4], [16]. Since the simulations are analyzed mainly from the induced junction b-Si photodiode perspective, the n-type bulk doping concentration is set to 2.5×10^{11} cm^{-3} similar to [4]. This allows direct comparison of the model with experimentally demonstrated equivalent. The simulations are done using Silvaco Atlas [17] and full details on all used parameters and physics models are given in Appendix A.

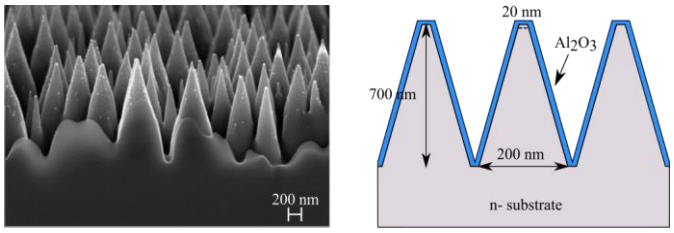

Fig. 1. a) A scanning electron microscope (SEM) image of a typical b-Si nanostructure coated with ALD Al_2O_3 that is used as a basis for the modeled structure. b) A schematic of the structure for which the model is developed. The structure consists of triangular silicon spikes (200 nm wide and 700 nm high with 20 nm wide tip) coated with a conformal thin film. As a starting point, a 20 nm thick Al_2O_3 layer and lightly phosphorus-doped silicon bulk are used, similar to the structure studied in [4]. The bulk extends 2 µm below the needles. The drawing is not in scale.

B. Electric Field and Charge Carrier Distribution

Investigation of the field-effect in b-Si is started by modeling electric field and carrier concentration in b-Si covered with ALD Al_2O_3. The electric field and the resulting carrier distribution below ALD Al_2O_3-coated b-Si are likely affected by the morphology of the nanostructure, since the nanometer-scale structures are surrounded by charges at all directions. Although not necessarily essential for surface passivation, the direction of the electric field is important for photodiode operation, since it affects the collection of light-generated charge carriers. Also in the FFE design of IBC cells, the electric field direction has an effect on the transport of minority carriers within the front emitter region.

To investigate the effect of b-Si morphology on electric field and the resulting charge carrier distribution inside and in the vicinity of the b-Si needles, the hole concentration distribution in the 2 µm deep layer from the surface is simulated in the structure presented in Fig. 1b. The simulated hole concentration profile inside b-Si and within the first 500 nm of the bulk is shown in Fig. 2a. In the entire shown region, the hole concentration exceeds the n-type bulk dopant concentration by several orders of magnitude. Hence, the entire b-Si needles and more than 500 nm of bulk below the nanostructures are inverted into p-type, which confirms that the charges at the Si-Al_2O_3 interface induce a strong junction at the b-Si surface with the applied parameters.

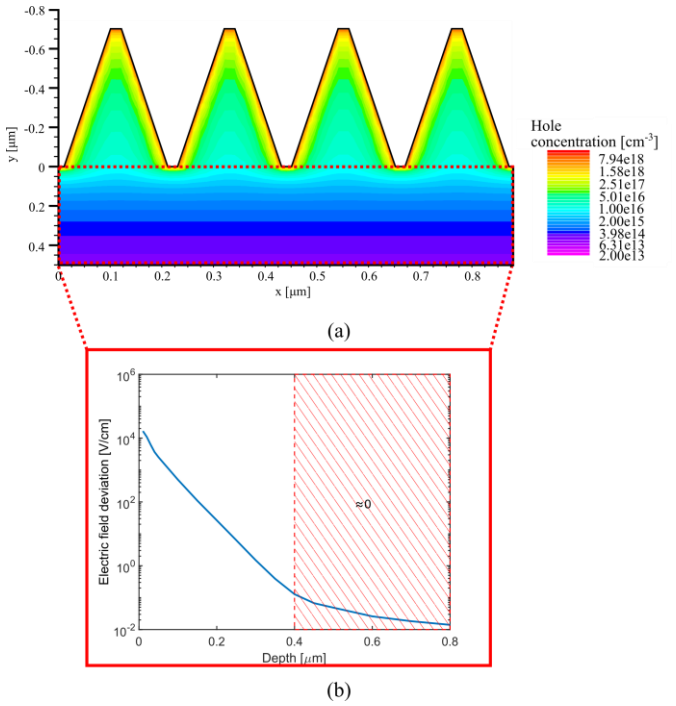

Fig. 2. a) Simulated concentration distribution of holes in b-Si needles. b) Standard deviation of the corresponding electric field in horizontal cross-sections below b-Si as a function of depth. Note the logarithmic y-axis. Only the first 800 nm of the bulk is presented, although the simulation was extended to 2 µm depth from the bottom of the b-Si nanostructures.

The hole concentration profile in Fig. 2a reveals that the electric field in b-Si is laterally non-homogeneous, as expected. Therefore, the lateral non-homogeneity of the electric field is investigated by taking horizontal cross-sections from the simulated electric field starting from the bottom of the b-Si needles (y = 0 µm in Fig. 2a) and progressing towards the bottom of the simulated bulk region with new cross-section taken every 50 nm. Standard deviation of the electric field magnitude is calculated for each cross-section and plotted as a function of depth in Fig. 2b

The figure shows that the deviation in electric field decreases exponentially in the bulk and reaches practically zero (deviation decrease comparable to 10^{-5}, default convergence threshold in Atlas) 400 nm below the bottom of the b-Si nanostructures. Consequently, the electric field can be considered flat starting from that depth. With higher bulk doping, the field-effect would reach a shorter distance in the bulk. This is in analogous to a doped p-n junction, where the electric field extends deeper into the side with lower doping. Hence, also from this perspective, an induced junction b-Si photodiode is a challenging example due to the low substrate doping.

The result indicates that ALD Al_2O_3-coated b-Si with bulk resistivity typical for photodiodes can be modelled using a planar equivalent from the electric-field perspective as long as the charge carriers of different type are collected, i.e., the induced junction extends, at least 400 nm below the b-Si needles, where the electric field is already flat. For long-wavelength radiation, which is absorbed deep in the substrate, the situation is naturally analogous to the planar case: when the electric field is flat at the junction, it is flat also deeper in the bulk. Instead, short-wavelength photons create electron-hole pairs within the induced region. Nevertheless, the generated minority carriers (i.e., electrons) are repelled from the surface due to the strong electric field induced by the negative charges, and the low doping concentration of the material ensures that the charge carriers are effectively collected by the flat junction.

C. Effect of Substrate Doping on Inversion Depth

The above section concluded that the field-effect in b-Si can be simulated using a planar equivalent model as long as the induced inversion layer extends deep enough in the bulk below the nanostructures, where the lateral non-homogeneity in the electric field is diminished. To study how sensitive the inversion depth, and hence the planar model, is to material parameters, the electric field simulation is repeated with varying bulk doping concentrations, while keeping the dielectric charge density constant. Simultaneously, the edge of inversion layer, i.e., the depth at which the hole concentration exceeds the bulk dopant concentration, is monitored. Since the simulation concentrates only on phenomena inside the b-Si needles, the accuracy of the simulation is increased by using a structure consisting of only a single cylindrically-symmetric b-Si needle.

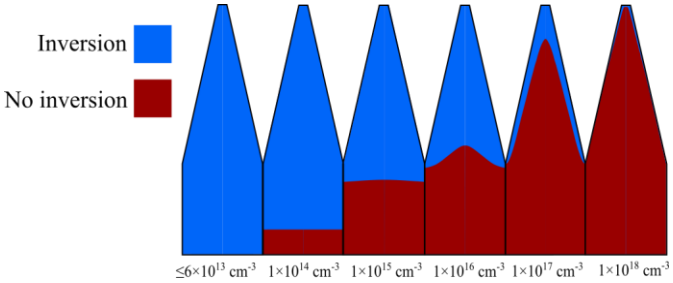

Fig. 3. Inverted (blue regions) and non-inverted (red regions) regions of b-Si needles and 400 nm bulk below them with different n-type dopant concentrations between 6×10^{13} cm^{-3} and 1×10^{18} cm^{-3}, while charge density on the surface is kept at -2.5×10^{12} cm^{-2} typical for ALD Al_2O_3.

Fig. 3 shows the evolution of the inversion layer edge in b-Si needles with increasing dopant concentration. The whole b-Si needle and 400 nm of bulk below the nanostructures is inverted with n-type dopant concentration of 6×10^{13} cm^{-3} or lower (i.e., resistivity of >74 Ωcm). When increasing the doping level, horizontal variations appear below the needle. The needle starts to have non-inverted regions when the dopant concentration exceeds ~1×10^{16} cm^{-3}, which is close to a typical doping level for solar cell substrates. Hence, an induced FFE can likely be realized in IBC cells by an ALD Al_2O_3 thin film deposited on the front, as long as the substrate resistivity is kept above ~1 Ωcm. However, non-lateral electric field components may have an effect on carrier transport within the induced region already with that resistivity. Elimination of the variations in electric field direction would require a higher charge density on the surface. The entire needle remains non-inverted with doping concentration higher than 1×10^{18} cm^{-3} (~26 mΩcm).

Based on Fig. 3, we can conclude that ALD Al_2O_3-coated b-Si can be approximated with a planar surface as long as the bulk dopant concentration is 6×10^{13} cm^{-3} at the maximum, after which the inversion region does not reach the distance with no horizontal variations in the electric field. This distance was found to be almost independent on dopant concentration. The field flattens around 400 nm below the b-Si needles with all the

studied dopant concentrations below 1×10^{17} cm^{-3}. With 1×10^{17} cm^{-3} and higher doping levels the inversion layer is so shallow that the electric field flattens already inside the needle. The presented case applies to a typical dielectric charge density for ALD Al_2O_3 [5]. Higher charge densities would result in stronger inversion, enabling inversion formation with higher substrate doping concentrations. Correspondingly, the opposite applies for lower charge densities. Hence, the model is directly applicable to photodetectors with low substrate doping concentration, while the accuracy for e.g. solar cells that typically have higher bulk doping concentration can be improved by selecting a dielectric with a higher charge density than in Al_2O_3.

D. Effective Charge Density in the Dielectric Film

The above results indicate that a planar surface can be a valid approximation of thin film-coated b-Si, when the charge density and substrate doping are within certain boundaries. What is still missing from the planar model is to find the correct charge density to be applied on a planar surface to induce equally strong field-effect as observed in b-Si.

Experimental studies [4], [5], [18], [19] have reported effectively three to seven times higher charge densities on b-Si compared to planar surfaces coated with an identical dielectric thin film, which affects the electric field strength in the b-Si structures. Based on experiments and analytical one-dimensional calculations, von Gastrow et al. [5] deduced that the charge enhancement factor for b-Si is directly proportional to the increased surface area with respect to a flat surface. With the introduced cylindrically-symmetric b-Si model, we expand the analysis into 3D and investigate if the ratio of surface areas can be used directly as the charge density enhancement factor in our planar model. As a clarification, the term effective charge density refers here to the density of charges that is needed on a planar surface to induce equally strong electric field as on b-Si, and not simply how much charge there is per surface area.

As can be seen from Fig. 2, the electric field profile in b-Si differs significantly from that in material with a planar surface. Thus, it is not possible to determine the effective charge density directly by comparing the electric field distributions in the vicinity of b-Si and planar surfaces. On the other hand, the influence of the electric field is seen as the number of holes the field attracts into the inversion layer. Consequently, the electric field and the effective charge density are interlinked here for the model by the average hole concentration in the inversion layer, which allows a direct comparison between b-Si and planar surfaces. This is done by integrating the hole concentration along vertical cross sections of a b-Si needle. The entire needle area is covered by repeating the integration in 10 nm intervals and integrating the results in horizontal direction (inset in Fig. 4). This yields the total number of holes in the needle, which is divided by the integrated surface area to obtain the average hole concentration. The same procedure is repeated with a planar structure with varying charge densities in the dielectric.

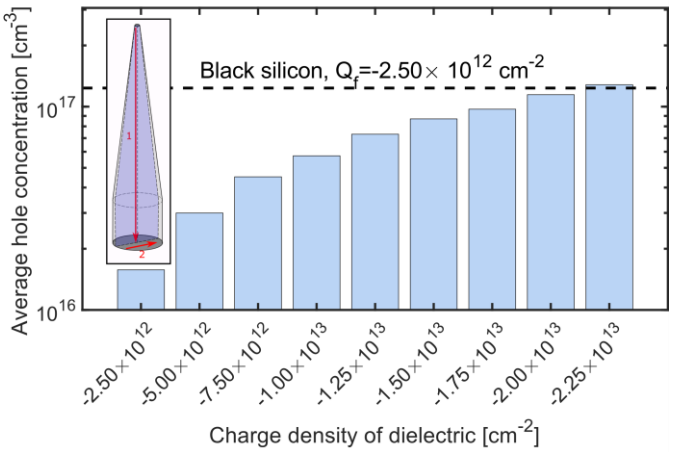

Fig. 4. Average hole concentration on a planar and a b-Si surface. The dashed black line represents the average hole concentration in the volume of a single b-Si needle and 1 µm of bulk silicon below it when a charge density of -2.5×10^{12} cm^{-2} is applied to the needle surface with typical n-type bulk resistivity for photodetectors. The blue bars indicate the corresponding average hole concentrations near a planar surface with varying charge densities. The inset illustrates the directions and area of the integrations. Note the logarithmic y-axis.

In Fig. 4, the blue bars indicate the average hole concentration resulting from the planar model with different dielectric charge densities, whereas the black dashed line indicates the corresponding value for the ALD Al_2O_3-coated b-Si structure. In the planar model, the average hole concentration increases approximately linearly as a function of the applied charge density (note the logarithmic y-axis in Fig. 4). The values for planar and b-Si surfaces match, when approximately nine times higher charge density is applied (-2.25×10^{13} cm^{-2}) to the planar surface compared to b-Si. This indicates that the effective charge density on b-Si is nine times higher compared to a planar surface with identical dielectric. Hence, a nine times higher charge density value should be used in simulations, when b-Si is approximated with the planar model.

The factor nine is slightly larger than the experimentally determined charge enhancement factors. Additionally, it is not directly proportional to the increase in surface area, as has been previously speculated [5], since the simulated needle has only seven times larger surface area compared to the planar structure. The difference between simulated and experimental values is most likely caused by the ideal needle shape used in the simulations. Asymmetry and the randomness in the size and shape of a real b-Si structure affect the achievable enhancement factor.

In summary, the following two aspects need to be considered in the planar model for b-Si: i) the combination of bulk resistivity and charge density at the Si-dielectric interface should be such that the inversion region extends sufficiently far below the b-Si needles (400 nm in the demonstrated case) so that no lateral variations occur in the electric field, and ii) the enhancement of inversion strength should be taken into account by multiplying the charge density on a planar surface with an enhancement factor, which depends on the b-Si geometry. If the substrate doping density and/or charge density of the dielectric film are drastically changed, point i) needs to be re-validated and the enhancement factor needs to be redefined. If only the

geometry of the b-Si changes, the enhancement factor is the sole parameter needing readjustment.

III. Black Silicon Device Modeling

A. Device structure and Simulation Parameters

After developing the planar model for b-Si, it is applied to device-level simulations. The device with the most demanding requirements for the field-effect, i.e., an induced junction b-Si photodiode, is selected here as an example. The device front surface consists of ALD Al_2O_3-coated b-Si on the photosensitive area in the center, surrounded by an anode contact metal ring. The rest of the front surface is covered with Al_2O_3, as indicated with blue in the figure. Backside of the device is covered with metal and forms the cathode contact.

The operation of the device is simulated using a structure shown in the inset of Fig. 5. The material parameters and dimensions are selected to agree with those used in the component that was experimentally demonstrated in [4]. The substrate is 525 µm thick, highly-resistive (>10 kΩ) n-type silicon corresponding to phosphorus dopant concentration of 2.5×10^{11} cm^{-3}. Charge carrier lifetime in the high-purity silicon is 10 ms. The photosensitive area in the middle is 2 mm wide, where b-Si is replaced with a planar surface using the principles discussed in Chapter 2. First, the substrate resistivity and charge density at the Si- Al_2O_3 interface are such that they fulfill the requirement of strong inversion 400 nm below the nanostructure bottom, where the electric field is flat with the applied resistivity and thin film charge (Fig. 3). Secondly, to get the effective charge density corresponding to the b-Si surface, the local charge density (-2.5×10^{12} cm^{-2}) is multiplied by a factor nine, as determined in Chapter 2.4. The distance between the 50 µm wide aluminum contacts and the chip edge is 0.5 mm. To form ohmic contacts, the substrate under the anode and the cathode is heavily doped with boron and phosphorous, respectively. The remaining areas of the top surface are covered with a 20 nm thick Al_2O_3 film. Appendix B contains further details on different parameters and physics models used in the Silvaco Atlas simulations of the described structure.

B. Verification of the Model: Comparison to Measured EQE

To verify the correctness and accuracy of the developed planar model, the internal quantum efficiency (IQE) of the photodiode is simulated and compared to experimental data measured from an induced junction b-Si photodiode [20]. The IQE is simulated by applying a 2 mm wide light beam with a 10 mW/cm^2 power density perpendicular to the active area, similar to the actual measurement, and simulating the output current. Excellent chemical surface passivation from the Al_2O_3 is assumed by setting the surface recombination velocity (SRV) of electrons (S_n) and holes (S_p) both to 1×10^5 cm/s [21] on all Si- Al_2O_3 interfaces. Since the IQE cannot directly be measured from actual components, the comparison between simulated and experimental performance is done as external quantum efficiency (EQE). Hence, the simulated IQE is multiplied by experimental absorbance data measured from a b-Si sample to calculate the EQE.

Fig. 5 shows the simulated EQE of the photodiode as a function of wavelength along with an EQE spectrum measured from an actual induced junction b-Si photodiode. The quantum efficiency is simulated only for wavelengths above 400 nm in order to maintain high accuracy. The accuracy of device-level simulations for short wavelengths is limited by inaccuracy in modeling of light absorption due to the limited number of mesh elements in the Silvaco Atlas model close to the surface, where the ultraviolet photons are absorbed. The field-effect model presented in Section 2 is applicable also closer to the front surface. Hence, the accuracy for wavelengths shorter than 400 nm could be improved by setting the generation profile of charge carriers based on optical simulation of b-Si as an input [22],[23]. Since the EQE of the selected experimental photodiode is high at a very wide wavelength range, the comparison of its EQE spectra to the simulated equivalent is highly sensitive to any possible inaccuracies in the simulation model. Hence, the selected device is highly suitable for the verification of the developed planar model. Fig. 5 shows that the simulation model in general accurately predicts the EQE with <1% difference up to 1050 nm, which verifies that the introduced planar model for b-Si is valid.

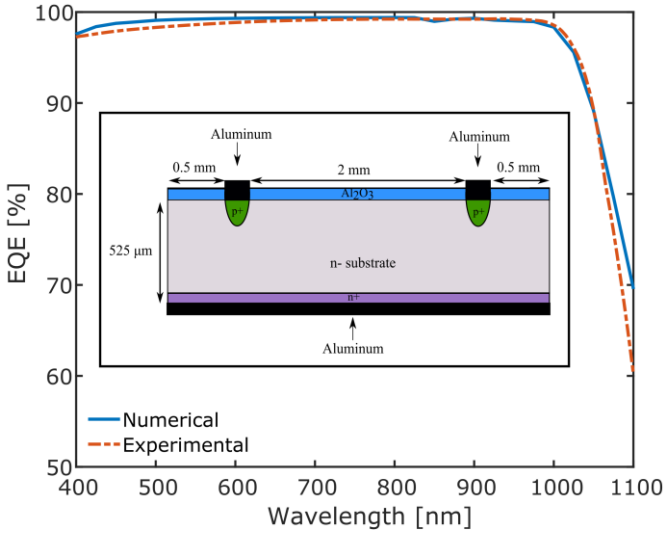

Fig. 5. Comparison of simulated (solid blue line) and experimental (dashed red line) EQE spectra of induced junction b-Si photodiode verifying the validity of the proposed model. Inset shows a schematic of the structure used to model the operation of the photodiode. The silicon substrate (gray area) is of high resistive n-type material and 525 µm thick. The entire backside is doped with phosphorous and covered with aluminum to form the cathode contact. The 2 mm wide active area on front side is surrounded with boron doped and aluminum covered anode contacts. The rest of the front surface is covered with 20 nm thick Al_2O_3 film and its fixed charge generates the induced junction. Drawing is not in scale

C. EQE With Different Dielectrics

After validating the planar model for b-Si photodiodes, it can be conveniently used to optimize the device and process parameters. One critical parameter for the device performance is the quality of the interface between silicon and the dielectric, which is described by SRV of charge carriers. The parameter can vary significantly depending on the chosen dielectric and the process parameters [24]. To demonstrate one potential application for the developed model, it is utilized to study how variation in SRV affects the b-Si photodiode performance. For these simulations, the effective charge density applied on the device surface is reduced to a level typically found in thermally-grown silicon dioxide (SiO2, -1×10^{11} cm^{-2}) [25], which is conventionally used in silicon photodiodes. The chosen charge

level is high enough to fulfill the requirements defined in Chapter 2 and hence the planar model for b-Si can be used.

Fig. 6a shows the simulated EQE spectra with varying S_n and S_p applied to the Si-dielectric interface on the front. Surface recombination has a relatively small influence on EQE in the long wavelength region (>800 nm), since long-wavelength photons generate charge carriers mostly deep in the bulk, where the front surface has a negligible effect. However, surface recombination starts to have an impact on EQE at wavelengths shorter than 700 nm, since the short-wavelength photons generate carriers close to the front surface. Nevertheless, the effect of front surface recombination is overall rather negligible between $S_p=S_n=0$ and $S_n=S_p=1\times10^5$ cm/s, and a noticeable reduction in EQE is seen only with higher recombination velocities.

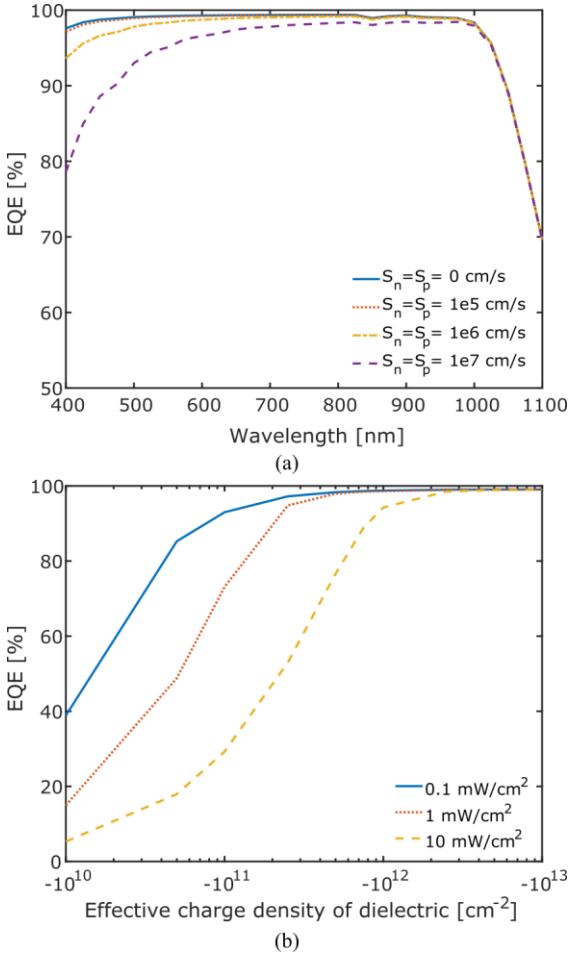

Fig. 6. a) Simulated EQE spectra with a constant effective charge density (-1×10^{11} cm^{-2}) and illumination intensity (10 mW/cm^2) and front surface recombination velocity between 0 and 10^7 cm/s. b) EQE at a 500 nm wavelength as a function of effective charge density at the Si-dielectric interface, when the device is illuminated with varying light beam intensities. S_p and S_n are set to 1×10^7 cm/s to represent the worst-case scenario.

It is worth noting that the S_p and S_n parameters cannot directly be compared to the effective values (S_{eff}) obtained by typical characterization methods, such as surface photovoltage or photoconductance decay. Instead, the S_p and S_n discussed here are the fundamental surface recombination velocities of electrons and holes caused by trap states in the bandgap. Here, 1×10^5 cm/s corresponds to a surface with excellent chemical passivation obtained with SiO_2 or Al_2O_3 [21], whereas 1×10^7 cm/s represents a highly recombining silicon-metal interface [26].

Based on Fig. 6a, it can be concluded that even relatively low effective charge density, such as typically found in thermal SiO_2, may result in a surprisingly high EQE as long as the surface is chemically well passivated, i.e., the SRV is low. On the contrary, poor passivation results in significantly reduced performance especially in the UV region. Similar simulations were repeated also with an effective charge density comparable to ALD Al_2O_3 on planar surface (-2.5×10^{12} cm^{-2}), in which case S_p and S_n had a negligible effect on EQE throughout the inspected wavelength region. Hence, a higher effective charge density is preferred to reduce the sensitivity of the device performance on surface quality.

In addition to SRV, another parameter that can be controlled by the selection of the dielectric material and its deposition process is the charge density at the surface. For instance in ALD-grown dielectrics, the resulting charge density is sensitive to several parameters, such as used precursors [19], surface pre-treatment [27], and post-deposition anneal [28]. Consequently, the developed model is next applied to investigate, how large impact a change in the effective charge density has on the photodiode performance. The device EQE is inspected at the wavelength of 500 nm, since it is short enough to be greatly affected by surface recombination, while the penetration depth is still deep enough so that the limited surface mesh resolution close to the surface has no effect on the result. The surface recombination velocities on the Si-dielectric interface are set to $S_n=S_p=1\times10^7$ cm/s to represent the worst-case scenario. Additionally, light intensity is varied to investigate the injection level dependency of the response. A higher number of injected carriers generated by more intense illumination weakens the inversion, which emphasizes the effect of surface recombination.

Fig. 6b shows the EQE at the selected wavelength as a function of the effective dielectric charge density under different illumination intensities. The figure shows that with a large effective dielectric charge density (>2×10^{12} cm^{-2}), surface recombination and illumination intensity have practically no effect on device performance, resulting in near unity EQE. Instead, when a lower effective charge density is applied, the EQE is impaired significantly by increased light intensity.

The behavior of EQE as a function of light intensity can be explained by the sheet resistance of the inversion layer. Illumination generates charge carriers, which propagate in the inversion layer. However, the flow of the photogenerated current is hindered by the sheet resistance of the inversion layer, which causes ohmic losses and generates a potential difference, i.e., forward-biases the photodiode. The forward bias weakens the inversion and shrinks the depletion region, resulting in a lower EQE. Moreover, the sheet resistance is proportional to carrier concentration in the inversion layer, and hence, directly dependent on the effective charge density of the dielectric, as indicated in Fig. 4. Thus, a lower effective charge density results in higher sheet resistance, which in turn causes stronger forward-biasing and lowers the EQE. Moreover, higher light intensity results in larger photocurrent, and thus, in higher forward bias, which further decreases the EQE.

This all means that the effective charge density of the dielectric directly defines the dynamic range of the photodiode, i.e., the range where the EQE remains independent of the illumination intensity. Fig. 6b indicates that the magnitude of the effective charge density should be at least 2×10^{12} cm^{-2} to expand the dynamic range in UV. Nevertheless, the lower limit for the effective charge density can likely be relaxed as long as surface recombination is properly handled.

IV. CONCLUSIONS

In this work we investigated the field-effect in dielectric-coated b-Si and developed a model where the b-Si can be approximated with a planar surface on two conditions: i) an inversion layer induced by the charges needs to reach far enough below the b-Si needles so that the electric field has no lateral variations at the depth of the junction, and ii) the charge density of the dielectric applied to the planar surface needs to be adjusted so that it takes into account the field enhancement caused by the geometry of b-Si. These principles are applicable to any device that utilizes charge-induced field-effect. In this work, we demonstrated as an example that the electric field flattens 400 nm below typical b-Si nanostructures resulting from an ICP-RIE process in cases where the substrate phosphorous dopant concentration is below 1×10^{17} cm^{-3} and charge density corresponds to typical ALD Al_2O_3. Closer inspection revealed that the inversion layer reaches the flat electric field region, fulfilling the first condition, while the dopant concentration is less than 6×10^{13} cm^{-3}. With this particular b-Si morphology, the effective charge density enhancement factor was found to be approximately nine, suggesting that the factor is not directly proportional to the increase in surface area. The described method could be used also to study different b-Si morphologies in order to find the optimal structure yielding the highest enhancement factor, and hence, the largest field-effect enhancement.

The developed planar model was then applied to simulate the QE of an induced junction b-Si photodetector. The same principles could be applied also to other b-Si morphologies and devices, including solar cells. The model was validated by comparing the simulated QE with experimental results from an identical device. Less than 1% difference occurred between the simulated and experimental QE with wavelengths below 1050 nm. Finally, the model was utilized to study, how variation in critical device parameters, such as SRV and the effective charge density of the dielectric, affect the photodiode performance. The simulations demonstrated that with low effective charge density, the short wavelength response is strongly dependent on surface recombination and illumination intensity. On the other hand, the parameters had practically no impact on EQE when high effective charge density was applied.

APPENDIX

A. Simulation Parameters Used in the Black Silicon Model

The black silicon structure is constructed using DevEdit, the device structure editor included in the Silvaco TCAD framework. The simulation begins by defining the structure shown in Fig. 1b. Mesh for the constructed structure is generated using the automated meshing tool included in DevEdit. Preliminary electric field simulated with a coarse mesh is used as an input to the meshing tool and it then adjusts the size of the mesh elements based on the electric field. The element density is increased in areas with large changes in the field. The actual simulations are then performed with Atlas using the defined structure and mesh. For some of the simulations a modified version of the model was used which includes only one silicon needle but allows the usage of cylindrical symmetry. All other parameters are the same than in the four-needle model.

The n-type dopant concentration in silicon areas is set to 2.5×10^{11} cm^{-3} and fixed charge of -2.5×10^{11} cm^{-2} is applied to all interfaces between silicon and Al_2O_3. For consistency, the simulations also include the same additional recombination, carrier statistics, mobility, and bandgap narrowing physics models as the photodiode model (see Appendix B).

B. Simulation Parameters Used in the Black Silicon Photodiode Model

First, the structure show in the inset of Fig. 5 is defined in Atlas with a coarse mesh. Preliminary electric field simulation done with the coarse mesh is then used as an input for the automatic meshing tool of DevEdit which adjusts the size of the mesh elements based on changes in the electric field. Finally, the refined mesh is used for the simulations done with Atlas.

The n-type dopant concentration in all silicon areas is first set to 2.5×10^{11} cm^{-3}. The typical charge density found in ALD Al_2O_3 (2.5×10^{12} cm^{-2}) is multiplied with the b-Si enhancement factor of nine and then applied to the Si- Al_2O_3 interfaces. The dopant profiles of the implanted n and p-type areas under contacts are simulated with ICECREM and then imported into the Atlas simulation model. The areas with aluminum are defined as ideal ohmic contacts. In addition to the default physics models used in Atlas, several models are included. For better charge carrier recombination modeling Shockley-Read-Hall (SRH) and Auger recombination models are added. SRH carrier lifetime in the bulk silicon is set to 10 ms. For the used substrate resistivity, we calculated corrected Auger recombination coefficients of 3.919×10^{-30} cm^6/s (for electrons) and 8.415×10^{-31} cm^6/s (for holes) using equations given in [29]. The simulation also takes into account surface recombination occurring at the interfaces of different materials. On silicon-aluminum interfaces, the S_n and S_p are both set to 1×10^7 cm/s [26]. Instead, on Si- Al_2O_3 interfaces, S_n and S_p values are varied to investigate the effect of different surface passivation qualities. The default Maxwell-Boltzmann carrier statistics are replaced with the Fermi-Dirac statistics, which yield more accurate results for highly-doped regions. Furthermore, parallel electric field-dependent mobility is used to take into account the carrier velocity saturation in areas with strong electric fields. Carrier-carrier scattering for low-field mobility is used to add temperature, doping, and carrier-carrier scattering dependency to the mobility in regions with weak electric fields. Finally, bandgap narrowing is included using Slotboom formulation. More detailed description of each model and their implementation in Atlas can be found in [17].

The spectral response simulations were performed using the Luminous simulation package included in Atlas. To illuminate the device, a 2 mm wide light beam with 0.1 mW/cm^2 power density is defined at the center of the active area perpendicular

to it. The default refractive indices in the Atlas material database for Al_2O_3 and silicon are used in the light absorbance simulation. The refractive indices are used to calculate the charge carrier generation profiles in silicon using the 2D ray-tracer included in Luminous**.** The simulation is repeated while changing the beam wavelength at each iteration from 400 nm to 1100 nm with 25 nm steps. From the simulation data, we extract output currents from the contacts and available photocurrent (i.e. the current generated by photons that got absorbed in the device). These are used to calculate the IQE of the device. Using experimentally measured b-Si absorbance data IQE is converted into EQE.

The simulated structure has a planar surface and the light beam is perpendicular to it. Hence, the simulation does not take into account that the optical path in black silicon is increased due to scattering [22]. The longer optical path increases the amount of absorbed light when the wavelength is such that the absorption depth is longer than the substrate thickness (> 1050 nm). Therefore, the simulation accuracy might be affected when using wavelengths longer than 1050 nm.

REFERENCES

[1] P. B. Clapham and M. C. Hutley, "Reduction of lens reflexion by the 'Moth Eye' principle," *Nature*, vol. 244, no. 5414. pp. 281–282, 1973, DOI: 10.1038/244281a0.

[2] L. Sainiemi, V. Jokinen, A. Shah, M. Shpak, S. Aura, P. Suvanto, and S. Franssila, "Non-reflecting silicon and polymer surfaces by plasma etching and replication," *Adv. Mater*., vol. 23, no. 1, pp. 122–126, 2011, DOI: 10.1002/adma.201001810 .

[3] H. Savin, P. Repo, G. Von Gastrow, P. Ortega, E. Calle, M. Garin, and R. Alcubilla, "Black silicon solar cells with interdigitated back-contacts achieve 22.1% efficiency," *Nat. Nanotechnol*., vol. 10, no. 7, pp. 624–628, 2015, DOI: 10.1038/nnano.2015.89 .

[4] M. A. Juntunen, J. Heinonen, V. Vähänissi, P. Repo, D. Valluru, and H. Savin, "Near-unity quantum efficiency of broadband black silicon photodiodes with an induced junction," *Nat. Photonics*, vol. 10, no. 12, pp. 777–781, 2016, DOI: 10.1038/nphoton.2016.226.

[5] G. Von Gastrow, R. Alcubilla, P. Ortega, M. Yli-Koski, S. Conesa-Boj. A. Fontcuberta I Morral, and H. Savin, "Analysis of the Atomic Layer Deposited Al2O3 field-effect passivation in black silicon," *Sol. Energy Mater. Sol. Cells*, vol. 142, pp. 29–33, 2015, DOI: 10.1016/j.solmat.2015.05.027.

[6] P. Repo, A Haarahiltunen, L. Sainiemi, M. Yli-Koski, H. Talvitie, M. C. Schubert, and H. Savin, "Effective passivation of black silicon surfaces by atomic layer deposition," *IEEE J. Photovoltaics*, vol. 3, pp. 90–94, 2013, DOI: doi:10.1109/jphotov.2012.2210031.

[7] M. Otto, M. Kroll, T. Käsebier, R. Salzer, A. Tünnermann, and R. B. Wehrspohn, "Extremely low surface recombination velocities in black silicon passivated by atomic layer deposition," *Appl. Phys. Lett*., vol. 100, no. 19, pp. 1–5, 2012, DOI: 10.1063/1.4714546.

[8] J. Oh, H. C. Yuan, and H. M. Branz, "An 18.2%-efficient black-silicon solar cell achieved through control of carrier recombination in nanostructures," *Nature Nanotechnology*, vol. 7, no. 11. pp. 743–748, 2012, DOI: 10.1038/nnano.2012.166.

[9] J. Benick, A. Richter, R. Müller, H. Hauser, F. Feldmann, P. Krenckel, S. Riepe, F. Schindler, M. C. Schubert, M. Hermle, A. W. Bett, and S. W. Glunz., "High-Efficiency n-Type HP mc Silicon Solar Cells," *IEEE J. Photovoltaics*, vol. 7, no. 5, pp. 1171–1175, 2017, DOI: 10.1109/JPHOTOV.2017.2714139.

[10] A. R. Burgers, I. Cesar, N. Guillevin, A. A. Mewe, P. Spinelli, and A. W. Weeber, "Designing IBC cells with FFE : long range effects with circuit simulation," *2016 IEEE 43rd Photovolt. Spec. Conf*., pp. 2408–2411, 2016, DOI: 10.1109/PVSC.2016.7750073.

[11] P. Dong, Y. Zhang, H. Guo, C. Zhang, J. Ma, and X. Qu, "Efficient Low-Cost IBC Solar Cells with a Front Floating Emitter: Structure Optimization and Passivation Layer Study," *Energies*, vol. 11, no. 4, p. 939, 2018, DOI: 10.3390/en11040939.

[12] T. E. Hansen, "Silicon UV-Photodiodes Using Natural Inversion Layers," *Phys. Scr*., vol. 18, no. 6, pp. 471–475, 1978, DOI: 10.1088/0031-8949/18/6/025.

[13] L. L. Ma, Y. Zhou, N. Jiang, X. Lu, J. Shao, W. Lu, J. Shao, W. Lu, J. Ge, X. M Ding, and X. Y. Hou, "Wide-band 'black silicon' based on porous silicon," *Appl. Phys. Lett*., vol. 88, no. 17, 2006, DOI: 10.1063/1.2199593.

[14] Z. Huang, N. Geyer, P. Werner, J. De Boor, and U. Gösele, "Metal-assisted chemical etching of silicon: A review," *Adv. Mater*., vol. 23, no. 2, pp. 285–308, 2011, DOI: 10.1002/adma.201001784.

[15] C. H. Crouch, J. E. Carey, J. M. Warrender, M. J. Aziz, E. Mazur, and F. Y. Génin, "Comparison of structure and properties of femtosecond and nanosecond laser-structured silicon," *Appl. Phys. Lett*., vol. 84, no. 11, pp. 1850–1852, 2004, DOI: 10.1063/1.1667004.

[16] G. Dingemans and W. M. M. Kessels, "Status and prospects of Al2O3-based surface passivation schemes for silicon solar cells," *J. Vac. Sci. Technol. A Vacuum, Surfaces, Film*., vol. 30, no. 4, p. 040802, 2012, DOI: 10.1116/1.4728205.

[17] Silvaco Inc., "ATLAS User's Manual,", 2016, Accessed on: Nov. 28, 2019, [Online]. Available: https://dynamic.silvaco.com/dynamicweb/jsp/downloads/DownloadManualsAction.do?req=silentmanuals&nm=atlas

[18] T. Pasanen, V. Vähänissi, N. Theut, and H. Savin, "Surface passivation of black silicon phosphorus emitters with atomic layer deposited SiO2/Al2O3 stacks," *Energy Procedia*, vol. 124, pp. 307–312, 2017, DOI: 10.1016/j.egypro.2017.09.304.

[19] P. Repo and H. Savin, "Effect of Different ALD Al2O3 Oxidants on the Surface Passivation of Black Silicon," *Energy Procedia*, vol. 92, pp. 381–385, 2016, DOI: 10.1016/j.egypro.2016.07.116.

[20] M. Garin, J. Heinonen, L. Werner, T. P. Pasanen, V. Vähänissi, A. Haarahiltunen, M. Juntunen, and H. Savin, "Black silicon UV photodiodes achieve >130% external quantum efficiency," arXiv preprint arXiv:1907.13397 (2019)

[21] G. von Gastrow, P. Ortega, R. Alcubilla, S. Husein, T. Nietzold, M. Bertoni, and H. Savin, "Recombination processes in passivated boron-implanted black silicon emitters," *J. Appl. Phys.*, vol. 121, no. 18, pp. 0–7, 2017, DOI: 10.1063/1.4983297.

[22] A. J. Bett, J. Eisenlohr, O. Höhn, P. Repo, H. Savin, B. Bläsi, and J. C. Goldschmidt, "Wave optical simulation of the light trapping properties of black silicon surface textures," *Opt. Express*, vol. 24, no. 6, p. A434, 2016, DOI: 10.1364/OE.24.00A434.

[23] M. Kroll, T. Käsebier, M. Otto, R. Salzer, R. Wehrspohn, E. Kley, A. Tünnermann, and T. Pertsch, "Optical modeling of needle like silicon surfaces produced by an ICP-RIE process," *Photonics Sol. Energy Syst. III*, vol. 7725, p. 772505, 2010, DOI: 10.1117/12.854596.

[24] R. S. Bonilla, B. Hoex, P. Hamer, and P. R. Wilshaw, "Dielectric surface passivation for silicon solar cells: A review," *Phys. Status Solidi A*, vol. 214, no. 7, 2017, DOI: 10.1002/pssa.201700293.

[25] B. E. Deal, M. Sklar, a. S. Grove, and E. H. Snow, "Characteristics of the Surface-State Charge (Qss) of Thermally Oxidized Silicon," *J. Electrochem. Soc*., vol. 114, no. 3, p. 266, 1967, DOI: 10.1149/1.2426565.

[26] A. Fell, K. R. McIntosh, P. P. Altermatt, G. J. M. Janssen, R. Stangl, A. Ho-Baillie, H. Steinkemper, J. Greulich, M. Muller, B. Min, K. C. Fong, M. Hermle, I. G. Romijn, and M. D. Abbott, "Input parameters for the simulation of silicon solar cells in 2014," *IEEE J. Photovoltaics*, vol. 5, no. 4, pp. 1250–1263, 2015, DOI: 10.1109/JPHOTOV.2015.2430016.

[27] G. Dingemans, N. M. Terlinden, M. A. Verheijen, M. C. M. van de Sanden, and W. M. M. Kessels, "Controlling the fixed charge and passivation properties of Si(100)/Al2O3 interfaces using ultrathin SiO2 interlayers synthesized by atomic layer deposition," *J. Appl. Phys*., vol. 110, no. 9, p. 093715, 2011, DOI: 10.1063/1.3658246.

[28] J. Buckley, B. De Salvo, D. Deleruyelle, M. Gely, G. Nicotra, S. Lombardo, J. F. Damlencourt, P. Hollinger, F. Martin, and S. Deleonibus, "Reduction of fixed charges in atomic layer deposited Al2O3 dielectrics," *Microelectron. Eng*., vol. 80, pp. 210–213, 2005, DOI: 10.1016/j.mee.2005.04.070.

[29] A. Richter, S. W. Glunz, F. Werner, J. Schmidt, and A. Cuevas, "Improved quantitative description of Auger recombination in crystalline silicon," *Phys. Rev. B - Condens. Matter Mater. Phys*., vol. 86, no. 16, 2012, DOI: 10.1103/PhysRevB.86.165202.